https://doi.org/10.5194/acp-2020-975
Preprint. Discussion started: 20 October 2020

Atmospheric Chemistry and Physics Discussions

Modelling the impact of gas-phase pyruvic acid on acetaldehyde and peroxy radical formation in the boreal forest

Philipp G. Eger[1], Jan Schuladen[1], Nicolas Sobanski[1], Horst Fischer[1], Einar Karu[1], Jonathan Williams[1], Ville Vakkari[2,3], Jos Lelieveld[1] and John N. Crowley[1]

[1]Atmospheric Chemistry Department, Max-Planck-Institute for Chemistry, 55128-Mainz, Germany
[2]Atmospheric Composition Unit, Finnish Meteorological Institute, 00101 Helsinki, Finland
[3]Atmospheric Chemistry Research Group, Chemical Resource Beneficiation, North-West University, Potchefstroom, South Africa

Correspondence to: John N. Crowley (john.crowley@mpic.de)

Abstract.

Based on the first measurements of gas-phase pyruvic acid ($CH_3C(O)C(O)OH$) in the boreal forest, we derive effective emission rates of pyruvic acid and compare them with monoterpene emission rates over the diel cycle. Using a data-constrained box-model, we determine the impact of pyruvic acid photolysis on the formation of acetaldehyde (CH_3CHO) and the peroxy radicals $CH_3C(O)O_2$, CH_3O_2 and HO_2 during an autumn (IBAIRN) and summer (HUMPPA) campaign at the same site. The results are dependent on the photodissociation mechanism of pyruvic acid and we examine different scenarios in which the main photolysis products are either acetaldehyde or the $CH_3C(O)O_2$ radical, with different overall quantum yields. If CH_3CHO is taken to be the main product (as presently recommended by evaluation panels) we find that pyruvic acid photolysis can be a dominant source of this aldehyde in the boreal forest with a contribution of 79 % (IBAIRN) and 94 % (HUMPPA) and may help explain the high acetaldehyde levels observed during HUMPPA. On the other hand, if photolysis leads mainly to the formation of radicals, the emission of pyruvic acid has a profound impact on the rates of formation of peroxy radicals (with a contribution of ~20–50 %) and shifts the onset of radical production to earlier in the morning when actinic flux is dominated by wavelengths that are too long to initiate efficient ozone photolysis but which are absorbed by pyruvic acid.

1 Introduction

Organic acids play a crucial role in tropospheric chemistry, impacting secondary organic aerosol formation, air quality and climate (Kanakidou et al., 2005; Hallquist et al., 2009). Pyruvic acid ($CH_3C(O)C(O)OH$), an organic acid that is central in plant metabolism as part of the Krebs cycle (Walker, 1962), is found in tropospheric air in the gas phase as well as in the aerosol phase, especially in the boundary layer of vegetated regions. Gas-phase mixing ratios ranging from a few to several hundred parts per trillion (pptv) have been reported in various locations around the world, including the tropical rain forest,

https://doi.org/10.5194/acp-2020-975
Preprint. Discussion started: 20 October 2020


Atmospheric Chemistry and Physics Discussions

boreal forest, rural areas with temperate forest, and regions influenced by urban outflow. A recent overview of existing measurements of gas-phase pyruvic acid is given by Eger et al. (2020).

A major source of pyruvic acid is understood to be the photo-oxidation of isoprene, via the ozonolysis of methyl vinyl ketone and subsequent hydrolysis of the Criegee intermediates (Jacob and Wofsy, 1988; Grosjean et al., 1993; Paulot et al., 2009). Further potential sources are the photolysis of methylglyoxal (Raber and Moortgat, 1995), the gas-phase photo-oxidation of aromatics in the presence of NO_x (Grosjean, 1984; Praplan et al., 2014), the aqueous-phase oxidation of methylglyoxal (Stefan and Bolton, 1999) and reactions taking place within biomass burning plumes (Andreae et al., 1987; Helas et al., 1992). In addition, pyruvic acid has been reported to be directly emitted from vegetation (Talbot et al., 1990; Jardine et al., 2010a; Jardine et al., 2010b; Eger et al., 2020). Compared to acetic acid, the presence of a second (non-acidic) carbonyl group imparts on pyruvic acid an absorption spectrum that extends from ultraviolet to visible wavelengths (see Fig. 1) and photolysis is a major sink of pyruvic acid in the boundary layer, with deposition and heterogeneous uptake to the aerosol phase also contributing to its removal. Photolysis of pyruvic acid in air results in a number of different radical and stable products (see Fig. 1), the major ones being acetaldehyde, HO_2 and $CH_3C(O)O_2$ (more details are presented in Sect. 2.2.1). These products can have a significant impact on tropospheric chemistry, e.g. via the formation of peroxyacetyl nitrate (PAN), peracetic acid (PAA) and formaldehyde (HCHO).

Global models have recently revealed discrepancies between simulated and measured acetaldehyde concentrations (Millet et al., 2010; Wang et al., 2019; Wang et al., 2020). Wang et al. (2020) reported CH_3CHO mixing ratios that were up to a factor of 10 higher than global chemistry-transport model (EMAC) results in the marine boundary layer around the Arabian Peninsula, implying missing sources in remote and polluted regions. Wang et al. (2019) also found that models systematically underestimate CH_3CHO compared to observations in the remote troposphere, implying a missing source of acetaldehyde. This finding was supported by the simultaneous measurement of PAA (for which acetaldehyde is a precursor in remote environments) and by the organic aerosol source of CH_3CHO being insufficient to explain the results. Instead, Wang et al. (2019) suggested that CH_3CHO arises from the degradation of gas-phase organic compounds. Pyruvic acid, among other organic acids in the gas and aerosol phase, might be one of the compounds that transport and release acetaldehyde to the remote troposphere and its integration into global models might contribute to resolve discrepancies, especially in forested regions.

Generally, field measurements as well as modelling and laboratory-based kinetic studies on pyruvic acid are limited and its impact on atmospheric chemistry is still poorly understood. In this study we highlight the potential role of pyruvic acid in the boreal forest, one of the largest terrestrial biomes on Earth.

2 Experimental data and box model description

The goal of this study is to quantify the impact of pyruvic acid on acetaldehyde and radical formation rates by using a data-constrained, chemical box-model. For this purpose we make use of experimental data from two field studies, which were both performed in the Finish boreal forest at the “Station for Measuring Forest Ecosystem-Atmosphere Relations II” (SMEAR II)

https://doi.org/10.5194/acp-2020-975
Preprint. Discussion started: 20 October 2020


Atmospheric Chemistry and Physics Discussions

in Hyytiälä (61.846 °N, 24.295 °E, 180 m above sea level, see Hari and Kulmala (2005)), an area that is mainly characterised by large biogenic (monoterpene-dominated) emissions and low NO_x concentrations (Williams et al., 2011). An overview of the instruments used to measure trace-gases and other parameters relevant for this study is presented in Table S1 of the supplementary information.

2.1. The IBAIRN and HUMPPA campaigns

The IBAIRN campaign (Influence of Biosphere–Atmosphere Interactions on the Reactive Nitrogen budget) took place in September 2016, during the summer–autumn transition, and was characterised by frequent temperature inversions near ground level during night-time (Liebmann et al., 2018), which led to the accumulation of nocturnally emitted trace gases from vegetation. A detailed description of the campaign and the instrumental setup can be found elsewhere (Liebmann et al., 2018; Eger et al., 2020). Briefly, pyruvic acid was measured by a chemical ionisation quadrupole mass spectrometer with a detection limit (LOD) (10 s, 2σ) of 15 pptv (Eger et al., 2020). The sum of monoterpenes (henceforth referred to as MT) was measured by a PTR-ToF-MS and single monoterpenes were monitored by a GC-AED, described in detail by Liebmann et al. (2018). Despite some discrepancies related to instrument location and inhomogeneity in terpene emissions within the forest, both instruments were in reasonably good agreement throughout the campaign. Since we require a high temporal resolution for our simulation, we have used the PTR-ToF-MS dataset. Photolysis rate coefficients (J_{pyr}, J_{NO2}, $J_{O(1D)}$ and J_{HCHO}) were derived using actinic flux measurements from a spectral radiometer (METCON GmbH) and evaluated cross sections and quantum yields (Burkholder et al., 2015). Mixing layer (MXL) heights were derived by combining in-situ measurements made by a scanning Doppler lidar (Hellén et al., 2018) with results from the ECMWF ERA-Interim reanalysis (Dee et al., 2011) with a spatial resolution of ~80 km. Since the lidar was unable to resolve MXL heights < 60 m (as regularly experienced during nocturnal inversions), all values below this threshold have been set to 60 m, representing an upper limit.

The summertime boreal forest field measurement intensive HUMPPA-COPEC took place at the same location in July and August 2010 and was characterised by unusually warm temperatures for this time of the year with exceptionally large emissions from the biosphere. A detailed description of the campaign and meteorological situation can be found in Williams et al. (2011). Insights into HO_x and RO_x chemistry are presented by Crowley et al. (2018) who suggested that di-carbonyl compounds, including pyruvic acid, could help explain the high production rates of radicals necessary to explain the observations of H_2O_2 and PAA, especially during periods when the measurement site was impacted by biomass burning in Russia.

2.2 Box model description

The box model was developed with the goal of simulating the impact of pyruvic acid photolysis on formation rates of OH, HO_2, $CH_3C(O)O_2$, CH_3CHO, CH_3O_2, HCHO and CH_3OOH over several diel cycles during the two field campaigns in the Finish boreal forest described above. In all model runs, the parameters directly constrained by the observations were the temperature, pressure, relative humidity (RH), the gas-phase concentrations of O_3, NO, NO_2, PAN, CO and monoterpenes, as well as the photolysis rate constants $J_{O(1D)}$, J_{NO2}, J_{HCHO}, J_{HONO} and J_{pyr}. Depending on the campaign (IBAIRN or HUMPPA),

https://doi.org/10.5194/acp-2020-975
Preprint. Discussion started: 20 October 2020

Atmospheric Chemistry and Physics Discussions

other parameters were additionally constrained (see Sect. 2.2.2 and 2.2.3). A complete reaction scheme is listed in Table S2 of the Supplement. Rate coefficients were taken from the IUPAC evaluations (IUPAC, 2020). The atmospheric methane concentration was set to a constant value of 1.8 ppmv. Non-methane alkanes, the degradation of which represents ~ 30–45 % of the acetaldehyde source globally (Millet et al., 2010) were constrained to 1000 pptv of ethane, 250 pptv of propane and 150 pptv of n-butane, as found in similar environments in Finland (Hakola et al., 2006; Hellén et al., 2015).

For the box model, programmed in FACSIMILE code (Curtis and Sweetenham, 1987), three different scenarios were investigated, in which the pyruvic acid chemistry listed in Table S2 was modified (see below) in order to examine the sensitivity of the model output to photolysis quantum yields. The box model simulated the field data at 10 min temporal resolution.

2.2.1 Pyruvic acid loss rate and model scenarios

Photolysis and dry deposition are considered the dominant loss terms for gas-phase pyruvic acid, as reaction with OH is slow (1.2×10^{-13} cm^3 molecule^{-1} s^{-1} at 298 K) (Mellouki and Mu, 2003). Heterogeneous uptake to atmospheric aerosols is also calculated to be inefficient at this site, where particle surface area densities were of the order of 2×10^{-7} cm^2 cm^{-3} and the particles contained a large organic fraction (Liebmann et al., 2019) that is likely to reduce the uptake coefficient compared to that measured for purely aqueous particles ($\gamma = 0.06$, Eugene et al. (2018)).

In Fig. 1 we present the wavelength resolved photolysis rates across the UV-absorption spectrum of pyruvic acid (assuming the overall photolysis quantum yield is 0.2) and a scheme showing possible routes to formation of acetaldehyde and radicals following its photolysis. The three most important photolysis channels are:

$CH_3C(O)C(O)OH + h\nu \rightarrow CH_3COH + CO_2$ (R1, α_1)

$\rightarrow CH_3CO + HOCO$ (R2, α_2)

$\rightarrow CH_3C(O)OH + CO$ (R3, α_3)

where α_i are branching ratios with $\alpha_1 + \alpha_2 + \alpha_3 = 1$.

CH_3CO and HOCO react rapidly in air to form peroxy radicals:

$CH_3CO + O_2 + M \rightarrow CH_3C(O)O_2 + M$ (R4)

$HOCO + O_2 \rightarrow HO_2 + CO$ (R5)

The methylhydroxycarbene product of R1 (CH_3COH) is an unstable intermediate which can rearrange to form CH_3CHO (R6) with branching ratio β or react with O_2 to form HO_2 and CH_3CO (branching ratio 1-β), which via R4, results in formation of $CH_3C(O)O_2$.

$CH_3COH \rightarrow CH_3CHO$ (R6, β)

$CH_3COH + O_2 \rightarrow CH_3CO + HO_2$ (R7, 1-β)

The quantum yield of acetaldehyde formation (ϕ_1) is thus equal to $\phi\alpha_1\beta$, where ϕ is the overall quantum yield. The quantum yield of formation of $CH_3CO_3 + HO_2$ (via R1/R7 and R2) is $\phi\alpha_2 + \phi\alpha_1(1-\beta)$. Direct formation of $CH_3C(O)OH$ in R3 has a quantum yield of $\phi\alpha_3$.

https://doi.org/10.5194/acp-2020-975
Preprint. Discussion started: 20 October 2020

Atmospheric Chemistry and Physics Discussions

For the calculation of the pyruvic acid photolysis rate constant (J_{pyr}) and photolysis products we used different scenarios A–C that reflect the large variability in quantum yields and branching ratios reported in the literature. They are outlined in the following and summarised in Table 1 along with the dominant photolysis products in air. In scenario A, which represents a reference for the other scenarios, we assumed that the overall quantum yield for pyruvic acid photolysis (ϕ) is zero. As its reaction with OH is slow, setting J_{pyr} to zero effectively removes any contribution of pyruvic acid to acetaldehyde or radical generation. In scenario B we used pyruvic acid cross sections and quantum yields according to the UPAC recommendations (IUPAC, 2020), with an overall quantum yield of $\phi = 0.2$ and branching ratios $\alpha_1 = 0.6$, $\alpha_2 = 0.35$ and $\alpha_3 = 0.05$, favouring the formation of acetaldehyde. Scenario C is based on the quantum yields reported by Reed Harris et al. (2017) who suggest $\phi = 0.84$ with $\alpha_1 = 1$ and $\beta = 0.05$, i.e. only two relevant product channels forming mainly $CH_3CO_3 + HO_2$ (95%) and only low amounts of CH_3CHO (5%). The comparison of scenarios B and C illustrates the sensitivity of the model output to the chosen quantum yields and branching ratios. The plausibility of the scenarios is tested by comparing the results of our model runs with observations of acetaldehyde and PAA during HUMPPA.

The deposition rate of pyruvic acid was calculated from $k_{dep} = v_{dep}\ h_{MXL}^{-1}$ during day and $k_{dep} = 2\ v_{dep}\ h_{MXL}^{-1}$ during night (Shepson et al., 1992a), with the transition following the diel variation in the mixing layer height h_{MXL} (see Fig. S1 in the Supplement). Further, as the two trace-gases have similar solubilities, we assumed that the deposition velocity of pyruvic acid is equal to that of H_2O_2, so that $v_{dep} = 8.4$ cm s^{-1} during day and $v_{dep} = 0.8$ cm s^{-1} during night, as derived by Crowley et al. (2018) for the same site. This resulted in a minimum dry-deposition loss rate constant of $k_{dep} = 0.9 \times 10^{-4}$ s^{-1} during day and a maximum of $k_{dep} = 1.8 \times 10^{-4}$ s^{-1} during night.

2.2.2 IBAIRN simulation

The simulation was initiated on 05.09.2016 but we analysed the model output only in the period 09–21.09.2016, as high-resolution MT data was not available for the first campaign days. In addition to the parameters generally constrained in all model runs (see above), for IBAIRN the concentration of pyruvic acid was determined by the observations. The concentration of PAN, which is generally the most abundant of peroxy acetyl nitrates (PNs), was calculated from [PAN] = 0.9 × Σ[PNs] (estimation based on observations by e.g. Shepson et al. (1992b), Roberts et al. (2004) and Roiger et al. (2011)). OH was calculated from the correlation of ground-level OH measurements with UVB radiation intensity at the Hyytiälä site (Petäjä et al., 2009; Hellén et al., 2018) with $[OH] = 5.62 \times 10^5\ [UVB]^{0.62}$ molecule cm^{-3} when UVB is in units of W m^{-2}.

We added a constant value of 1.5 s^{-1} (accounting for unmeasured oxygenated VOCs) to the total OH reactivity (R_{OH}), so that the simulated OH concentration approximately matched the OH concentration derived from the UVB measurement.

2.2.3 HUMPPA simulation

The simulation was initiated on 14.07.2010, the output was only used from 21.07.–08.08.2010 due to missing PAN data at the beginning of the campaign. In addition to the parameters generally constrained in all model runs (listed above), for HUMPPA

https://doi.org/10.5194/acp-2020-975
Preprint. Discussion started: 20 October 2020


Atmospheric Chemistry and Physics Discussions

the concentrations of HCHO, HONO and CH_3CHO were determined by the observations. However, due to a lack of experimental data, we estimated the pyruvic acid concentration based on measured MT mixing ratios and the relationship between pyruvic acid and MT emission rates derived from the IBAIRN analysis (which is discussed later in Sect. 3.1). During HUMPPA, the site was impacted by a biomass burning plume on two occasions (26.07.–30.07.2010 and 07.08.–09.08.2010) and levels of CH_3CN, CO, PAN, H_2O_2, PAA and several oxidised organics were considerably enhanced over normal conditions. We present results both including and excluding the biomass burning periods.

3 Results and discussion

In the following, we discuss the model output for the IBAIRN and HUMPPA campaigns with a focus on pyruvic acid emission rates and its impact on acetaldehyde and radical chemistry in the boundary layer of the boreal forest.

3.1 Autumn campaign (IBAIRN): Pyruvic acid emission rate relative to monoterpenes

In order to quantify the pyruvic acid emission rate (E_{pyr}) during IBAIRN we assume that only photolysis and dry deposition contribute significantly to its overall loss rate (Sect. 2.2.1) and that pyruvic acid is in steady-state. The latter assumption is reasonable as its mean lifetime was (2 ± 0.5) h (for scenario B; shortest at night) and changes in the mixing ratio could reliably be reproduced by the simulation. Due to a homogeneous fetch at the measurement site we can neglect transport processes and E_{pyr} is defined by Eq. (1), where $[pyr]_{ss}$ is the measured concentration, J_{pyr} is the photolysis rate constant of pyruvic acid, k_{dep} is the first-order loss rate constant for its dry deposition, and h_{MXL} is the well-mixed boundary layer height.

$$E_{pyr} = [pyr]_{ss} \left(J_{pyr} + k_{dep}\right) h_{MXL} \quad (1)$$

E_{pyr} is effectively an emission rate normalised to the MXL height (h_{MXL}) and has units of pptv s^{-1} m. As the photolysis is a substantial fraction of the overall losses of $CH_3C(O)C(O)OH$, the choice of quantum yield ϕ (scenarios A, B and C) directly impacts the calculated emission rate. The same calculation is performed for the monoterpenes (E_{MT}) over the same period (and thus for the same MXL height). We note that h_{MXL} controls not only the value of k_{dep} but also directly affects the mixing ratios of both MTs and pyruvic acid for a given emission rate. The relative emission rate (E_{pyr} / E_{MT}) can be calculated from Eq. (2) where terms in square brackets are concentrations.

$$\frac{E_{pyr}}{E_{MT}} = \frac{[pyr]_{ss}\left(J_{pyr}+k_{dep}\right)}{[MT]_{ss}\left(k_{OH}[OH]+k_{NO3}[NO_3]+k_{O3}[O_3]\right)} \quad (2)$$

In the denominator, k_{OH}, k_{NO3} and k_{O3} are rate coefficients for reaction of monoterpenes with OH, NO_3 and O_3, respectively. An average lifetime of MT of (4 ± 2) h (largest at night), resulting from reactions with OH, NO_3 and O_3 (see Table S2), was calculated from the mean MT composition measured by GC-AED (49 % α-pinene, 13 % β-pinene, 27 % Δ-carene, 3 % Δ -limonene and 8 % camphene) and corresponding rate coefficients (Perring et al., 2013; Gaona-Colman et al., 2017; IUPAC, 2020).

https://doi.org/10.5194/acp-2020-975
Preprint. Discussion started: 20 October 2020


Atmospheric Chemistry and Physics Discussions

Note that the calculated emission rates are subject to substantial uncertainties arising from the measurement of pyruvic acid, MT, OH, O_3, NO_3, h_{MXL} and J_{pyr}. In particular, the results are very sensitive to the estimated deposition velocity (v_{dep}) of pyruvic acid which is an estimate based on the deposition velocity of H_2O_2 which itself has an uncertainty of ~ 90 % (Fischer et al., 2019). Further, our calculations are based on the assumption that the sources for pyruvic acid and MT emissions are evenly distributed and measurements made at ~ 8.5 m above the ground are representative of the entire boundary layer (i.e. that the boundary layer is well-mixed, including the very shallow boundary layer at night). A gradient in pyruvic acid mixing ratios at night cannot be ruled out, which would impact on our results. We estimate that the emission ratio (E_{pyr} / E_{MT}) in Eq. (2) is associated with an overall uncertainty of a factor ~2.

A time series of pyruvic acid and MT mixing ratios along with the MXL heigth (h_{MXL}) derived from a lidar measurement and from the ERA-Interim renanalysis is shown in Fig. S2 of the Supplementary Information. Whereas both MXL height datasets agree very well during the night when the MXL is shallow (usually < 100 m), the lidar data is on average a factor of ~2 lower during day and characterised by a much higher variability. For the derivation of the diel profile of h_{MXL} (Fig. S1) we took an average of both datasets. The diel variation displayed in Fig. S2, with highest MT mixing ratios at night, is characteristic for this boreal forest site and has been observed in earlier studies (Hellén et al., 2018).

In the following, we focus on the mean, diel profiles of E_{pyr}, E_{MT}, J-NO_2, T and h_{MXL} for the IBAIRN campaign, which are presented in Fig. 2. During September, the emission rate of pyruvic acid (E_{pyr}) reaches its maximum a few hours after solar noon when the temperature peaks, similar to E_{MT}. However, the amplitude of the day-to-night difference in E_{pyr} is a factor of ~3 smaller than observed for E_{MT}. This could indicate that pyruvic acid emissions are less temperature-dependent than MT emissions (see below) and that other environmental factors might additionally play a role at this time of year.

The emission rates of the MTs derived as described above show a large day-night variation with a factor ~20 larger values around noontime compared to midnight. This is significantly larger than the expected variation (factor 2–3) based on the average noon-to-midnight temperature difference of 10 K and the parameterisation of Guenther et al. (1993) whereby $E_{MT} \propto \exp(\beta(T - 297\ K))$ with $\beta = 0.1\ K^{-1}$ (which is in line in with the empirical value of $\beta = 0.12\ K^{-1}$ that was derived for this site in September by Hellén et al. (2018)). One potential reason for this discrepancy may be related to emissions in autumn from fresh leaf litter that significantly contribute to the observed mixing ratios (Hellén et al., 2018) and that the assumption of evenly distributed sources and a well-mixed boundary layer is not necessarily valid during night, especially during strong temperature inversions.

Fig. S3 in the Supplement shows that the daytime emission of pyruvic acid relative to MT (E_{pyr} / E_{MT}) varies by a factor of ~ 2, depending on the chosen scenario, whereas the nighttime emission ratio is only dependent on the deposition velocity of pyruvic acid. For further analysis we focus on the results from scenario B, using presently recommended photochemical parameters for pyruvic acid (IUPAC, 2020). On average (E_{pyr} / E_{MT}) ~ 0.6 with a minimum value of ~ 0.3 in the evening and a maximum value of ~ 1 in the early morning, indicating elevated pyruvic acid emissions relative to MT at night. To derive a *T*-dependent expression from the diurnal profile of the emission factor, we fit an exponential function to the plot of temperature versus E_{pyr} / E_{MT} (Fig. S4), yielding:

https://doi.org/10.5194/acp-2020-975
Preprint. Discussion started: 20 October 2020


Atmospheric Chemistry and Physics Discussions

$$E_{\mathrm{pyr}} = \left[0.28 + 3.17 \times \exp\left(\frac{273-T}{4.24}\right)\right] \times E_{\mathrm{MT}} \quad (3)$$

We note that (like the values of E_{pyr}) the temperature dependence derived is strongly influenced by the diel variation of the MXL height and thus carries significant uncertainty and may not be transferable to other locations or even times of the year.

As our measurements of pyruvic acid in the boreal forest are the first to have been made, we cannot compare our relative emission ratio (E_{pyr} / E_{MT}) with previous measurements in the boreal environment. Instead, where possible, we derive the emission ratio from measurements of MTs, isoprene and pyruvic acid in warmer climates. Jardine et al. (2010b) performed measurements in an enclosed (glass dome) tropical forest biome at Biosphere 2 in Arizona, US, where they found maximum concentrations of 120 ppbv isoprene, 6 ppbv monoterpenes and 15 ppbv pyruvic acid. As the glass dome absorbed actinic wavelengths and prevented active photochemistry, the chemical loss processes for pyruvic acid, isoprene, and MT (including photolysis and reactions with OH, O_3 and NO_3) are negligible. Initially disregarding the deposition of isoprene and MT, we derive lower limits of (E_{pyr} / E_{iso}) ~ 0.17 and (E_{pyr} / E_{MT}) ~ 4 (see Table 2). However, due to the presence of large concentrations of isoprene-consuming microbes in the soil of Biosphere 2, the isoprene loss rate via deposition may be enhanced, which will decrease the effective emission ratio (E_{pyr} / E_{iso}). In addition, branch enclosure studies were performed on a mangifera indica (mango) tree within Biosphere 2, yielding mean fluxes (in nmol m^{-2} s^{-1}) of 3.2 for isoprene, 0.09 for MT and 0.15 for pyruvic acid. Pyruvic acid emissions peaked during the day when temperature and photosynthetically active radiation (PAR) were highest and correlated very well with isoprene emissions and (to a certain extent) with MT emissions. Assuming that a mango tree is representative for the tropical vegetation, we derive emission ratio of (E_{pyr} / E_{iso} ~ 0.05 and (E_{pyr} / E_{MT}) ~ 1.7 (see Table 2), which is consistent with our estimations for the IBAIRN campaign. However, given that Talbot et al. (1990) observed great variability in pyruvic acid emission fluxes among five different tree species during measurements in the tropical Ducke Forest Reserve close to Manaus, Brazil, this agreement may, to some extent, be coincidental. Talbot et al. (1990) also reported a mean emission flux (derived from enclosure experiments) relative to isoprene of (E_{pyr} / E_{iso}) ~ 0.003, which is about one order of magnitude smaller than in the study of Jardine et al. (2010b). In a further branch enclosure study by Jardine et al. (2010a) emissions from a creosotebush (Larrea divaricata), which is typically found in US drylands, were investigated. Average noontime branch emission rates (in µg C gdw^{-1} h^{-1}) of 7.5, 10.4 and 0.2 for isoprene, MT and pyruvic acid resulted in relative emission ratios of (E_{pyr} / E_{iso}) ~ 0.05 and (E_{pyr} / E_{MT}) ~ 0.07 for this mixed isoprene-MT-emitting species.

The comparison with the few datasets available in the literature indicates that the variability of the emission factors (E_{pyr} / E_{MT}) and (E_{pyr} / E_{iso}) among different plant species and different environments is large. In addition, a lack of pyruvic acid measurements over different seasons in the boreal forest means that we cannot exclude that the value we derive is biased by emissions (e.g., from ground-level, decaying plant-litter in September) that are peculiar to this season and environment. The conclusions we draw from our following analysis are therefore relevant for the autumnal boreal forest but require validation before being extended to other regions and seasons with confidence.

https://doi.org/10.5194/acp-2020-975
Preprint. Discussion started: 20 October 2020

Atmospheric Chemistry and Physics Discussions

3.2 Contribution of pyruvic acid to acetaldehyde and radical formation

To quantify the impact of pyruvic acid photolysis during IBAIRN, we identified the relative contributions of the processes forming OH, HO_2, $CH_3C(O)O_2$, CH_3CHO, HCHO and CH_3OOH from our model runs, and compared scenario A (the reference run with no impact from pyruvic acid) with scenarios B and C. The campaign-averaged production rates are summarised in Table 3.

Figure 3 illustrates the relative importance of the various pathways to OH formation and the resulting OH concentrations for the three different scenarios. On average, the main source of OH radicals was the direct formation from O_3 photolysis (39 % in scenario B), followed by the reaction of HO_2 with NO (30 %) and O_3 + MT (25 %). The inclusion of pyruvic acid photolysis in the model increased the relative importance of the HO_2 + NO reaction by 1 % (scenario B) or 6 % (scenario C) due to increased HO_2 production. The overall OH production rate (13.1×10^5 molec cm^{-3} s^{-1} in scenario A, see Table 3) increases by 2 % in scenario B or 13 % when considering scenario C.

For HO_2 (Fig. 4) the three major sources during IBAIRN were the reactions OH + CO (39 %), RO_2 + NO (36 %), and CH_3O_2 + NO (19 %). In scenario B, pyruvic acid accounts for just 2 % of the total HO_2 production (via R2 and R5, see Fig. 1) whereas in scenario C this increases to 14 % (via R1 and R7). The overall HO_2 production rate (5.8×10^5 molec cm^{-3} s^{-1} in scenario A, see Table 3) increases by just 2 % in scenario B but by as much as 36 % in scenario C. Clearly, the combination of a high quantum yield of pyruvic acid photolysis and direct formation of radicals can have a significant impact on the HO*x* budget. As the photolysis of pyruvic acid occurs at wavelengths that are red-shifted compared to O_3 photolysis, the model predicts that the onset of photochemical radical formation in scenario C is about 1 hour earlier than without pyruvic acid photolysis.

Figure 5 summaries the results for $CH_3C(O)O_2$. The most important channel for $CH_3C(O)O_2$ production in Scenario A was by far the decomposition of PAN (95 %), followed by OH + CH_3CHO (5 %). When comparing scenario B with A, the overall $CH_3C(O)O_2$ production rate is slightly increased due to the presence of pyruvic acid, with a contribution of 8 % directly arising from its photolysis ($CH_3C(O)C(O)OH + h\nu$). In scenario C, the contribution from the photolysis of pyruvic acid increases to 52 % and the overall $CH_3C(O)O_2$ production rate almost doubles. This would make pyruvic acid an important source of $CH_3C(O)O_2$ during the IBAIRN campaign. In scenario C we also see a clear shift in the onset of radical generation to earlier in the morning when actinic flux is dominated by wavelengths that are too long to initiate ozone photolysis but are absorbed by pyruvic acid.

In the absence of pyruvic acid photolysis (scenario A), the production of acetaldehyde is dominated by the degradation of alkanes (n-butane, ethane, and propane). When including formation of CH_3CHO via pyruvic acid photolysis in scenario B (Fig. 6), the contribution of the alkanes drastically decreases, and pyruvic acid becomes the dominant source of acetaldehyde (79 %) in this environment. The fractional contribution remains high (53 %) in scenario C even though CH_3CHO is formed only at low yield (5 %) in this case. The pyruvic acid mixing ratios observed during IBAIRN would result in mean simulated acetaldehyde mixing ratios of ~115 pptv (Fig. 6d), which is reasonable for this site as shown in the HUMPPA dataset (Sect. 3.3).

https://doi.org/10.5194/acp-2020-975
Preprint. Discussion started: 20 October 2020


Atmospheric Chemistry and Physics Discussions

The three main sources of the CH_3O_2 radical in air are the reactions CH_4 + OH, $CH_3C(O)O_2$ + HO_2 and $CH_3C(O)O_2$ + NO, all preceding via formation of the CH_3 radical, in the last two cases a result of decomposition of the unstable intermediate CH_3CO_2. The CH_3O_2 radical is a source of both the most abundant aldehyde (HCHO) and methyl hydroperoxide (CH_3OOH) in the troposphere, the former preferentially formed at high NO_X levels, the latter under low NO_X conditions. As shown in Fig. 7, pyruvic acid photolysis increases the fraction of CH_3O_2 formed from $CH_3C(O)O_2$ to 5 % (scenario B) and 18 % (scenario C), with methane oxidation still accounting for most of the total production rate. In scenario C, the summed production rates of HCHO and CH_3OOH are increased by 42 % each (Table 3).

3.3 Summer campaign (HUMPPA): Contribution of pyruvic acid to acetaldehyde and $CH_3C(O)O_2$ formation

As pyruvic acid was not measured during HUMPPA, we use the calculated mean emission rate of pyruvic acid relative to MT during IBAIRN (derived from Eq. 2, see Table 1) as an input parameter for the HUMPPA simulation to estimate the pyruvic acid mixing ratios (in steady state) shown in Fig. 8.

Compared with IBAIRN, where [pyr] / [MT] ~ 0.3 on average, for HUMPPA the mean concentration ratio is ~ 1.6, which is mainly a consequence of the higher temperatures and larger MXL heights during the summertime HUMPPA campaign (especially at night) which result in lower pyruvic acid deposition rates. In addition, it is also influenced by the higher OH and O_3 levels in summer (HUMPPA) which contribute to MT losses. The highest pyruvic acid mixing ratios are modelled for the night-time (lowest h_{MXL}) and in periods impacted by biomass burning from Russia, which is indicated by elevated CO and HCN levels (periods highlighted in light blue). Coincidentally, the biomass burning periods were accompanied by high temperatures and high MT levels also. When excluding the biomass burning periods from the analysis, simulated pyruvic acid mixing ratios occasionally reach values up to ~ 2 ppbv with a mean campaign value of ~ 0.5 ppbv.

Similar to the autumn campaign IBAIRN we can now quantify the contribution of pyruvic acid photolysis to the formation of acetaldehyde, peroxy radicals and PAA. Therefore, we compare Scenarios A with B and C (as for the IBAIRN simulation in Sect. 3.2), in this case focussing on the $CH_3C(O)O_2$ radical and on acetaldehyde as both are precursors to $CH_3C(O)OOH$, which was measured during HUMPPA.

In the absence of pyruvic acid photolysis (Scenario A), the production of acetaldehyde is dominated by n-butane, ethane, and propane. However, these globally important CH_3CHO precursors are not sufficient to explain the acetaldehyde concentrations that were observed (Fig. 8). Another potential source is the direct biogenic emission from vegetation (see e.g. Rissanen et al. (2020), making up ~15 % of the total CH_3CHO source (Millet et al., 2010). However, on a global scale (and also in Finland) these emissions are a factor of ~5 smaller than the photochemical production term and have thus been neglected in the simulation. By enabling formation of CH_3CHO via pyruvic acid photolysis in Scenario B (see Fig. 9), the contribution of the alkanes reduces to 6 % and pyruvic acid becomes the dominant source of acetaldehyde (94 % in scenario B, 76 % in scenario C) during HUMPPA. Removing periods impacted by biomass burning plumes does not significantly change the overall conclusions (pyruvic acid contribution decreases by ~ 2 %). When comparing the time series of measured acetaldehyde mixing ratios with the model output (Fig. 8), we note that scenario B more closely reproduces the observations than scenario A which

https://doi.org/10.5194/acp-2020-975
Preprint. Discussion started: 20 October 2020


Atmospheric Chemistry and Physics Discussions

greatly underpredicts the observed CH_3CHO for much of the campaign. We conclude that pyruvic acid photolysis represents a potentially important contribution to acetaldehyde mixing ratios in the boreal forest and possibly also on a global scale (above forested regions).

The major source of acetylperoxy radical in Scenario A is the decomposition of PAN (93 %), with a minor contribution from the oxidation of acetaldehyde (7 %) (see Fig. 10). In Scenario B, the direct impact of pyruvic acid photolysis on $CH_3C(O)O_2$ is 3 %, whereas the indirect impact from the formation of acetaldehyde and its subsequent oxidation via CH_3CHO + OH is negligible. In contrast, in Scenario C, the direct contribution from the photolysis of pyruvic acid is 19 %, making pyruvic acid an important contributor to acetylperoxy radical generation in this environment and underlining the importance of dicarbonyls, as suggested by Crowley et al. (2018). However, the pyruvic acid mixing ratios alone (without other dicarbonyls) cannot explain the observed large PAA mixing ratios during HUMPPA (Crowley et al., 2018), especially during the biomass burning episodes.

4 Conclusions

Using pyruvic acid cross sections and quantum yields ($\phi = 0.2$) according to the IUPAC recommendations (scenario B in which the dominant photolysis products are CH_3CHO + CO_2), we identified pyruvic acid as an important source of acetaldehyde (CH_3CHO) in both autumn (IBAIRN) and summer (HUMPPA) with a contribution of 79 % respectively 94 % to the overall production rate. Pyruvic acid may thus have contributed to the source of elevated mixing ratios of acetaldehyde observed during HUMPPA which could not be explained by the degradation of alkanes. Our results might also help to explain the discrepancies between modelled and observed CH_3CHO mixing ratios in remote, forested regions where emissions of pyruvic acid may be significant. In contrast, under scenario B, the effect on OH, HO_2, $CH_3C(O)O_2$ and HCHO formation rates during both campaigns is minor (< 10%).

This picture changes drastically under scenario C, whereby the quantum yield is a factor of ~ 4 larger and formation of HO_2 and $CH_3C(O)O_2$ is preferred over CH_3CHO. In both campaigns pyruvic acid now increases the overall HO_2 production by ~ 20–35 % and the overall HCHO production by ~ 25–40 %. In scenario C, pyruvic acid photolysis is comparable to PAN decomposition as source of $CH_3C(O)O_2$ during IBAIRN, also shifting the onset of radical production to earlier in the morning. The presence of pyruvic acid can partly explain the elevated PAA mixing ratios observed in HUMPPA, though other oxygenates might play a role as well, especially during biomass burning events (Crowley et al., 2018).

In general, our results are strongly dependent on the chosen quantum yields and deposition velocities. To minimise the uncertainty in our calculations, there is an urgent need for further experimental work on the photochemistry of pyruvic acid. In addition, measurements of the deposition velocity of pyruvic acid in different environments are required to better constrain its lifetime and thus the impact of photolysis. Further, more enclosure studies will be necessary to investigate the dependence of pyruvic acid emission rates on different plant types and environmental conditions.

https://doi.org/10.5194/acp-2020-975
Preprint. Discussion started: 20 October 2020

Atmospheric Chemistry and Physics Discussions

Data availability

The Max Planck Institute data used for the IBAIRN analysis is archived with Zenodo at https://doi.org/10.5281/zenodo.3254828 (Crowley and Fischer, 2019). HUMPPA-COPEC-2010 data can be obtained on request (via John N. Crowley) from the owners.

Author contributions

PGE was responsible for the pyruvic acid measurement during IBAIRN and, with contributions from JNC and JL, ran the box model, analysed the model results for the IBAIRN and HUMPPA campaigns and wrote the manuscript. NS was responsible for the CRDS measurements of NO_2 and PANs during IBAIRN. JS was responsible for the O_3 and J-value measurements during IBAIRN. HF was responsible for the NO and CO measurements during IBAIRN and HUMPPA. EK and JW were responsible for the monoterpene measurements during IBAIRN. VV was responsible for the mixing layer height measurements during IBAIRN. All authors contributed to the paper.

Competing interests

The authors declare that they have no conflict of interest.

Acknowledgements

We thank the technical staff of SMEAR II station for the excellent support during IBAIRN and HUMPPA-COPEC.

Financial support

We are grateful to ENVRIplus for partial financial support of the IBAIRN campaign.

References

Andreae, M. O., Talbot, R. W., and Li, S. M.: Atmospheric measurements of pyruvic and formic acid, J. Geophys. Res. - Atmos., 92, 6635-6641, doi:10.1029/JD092iD06p06635, 1987.

Burkholder, J. B., Sander, S. P., Abbatt, J., Barker, J. R., Huie, R. E., Kolb, C. E., Kurylo, M. J., Orkin, V. L., Wilmouth, D. M., and Wine, P. H.: Chemical Kinetics and Photochemical Data for Use in Atmospheric Studies, Evaluation No. 18," JPL Publication 15-10, Jet Propulsion Laboratory, Pasadena, http://jpldataeval.jpl.nasa.gov., 2015.

Crowley, J. N., Pouvesle, N., Phillips, G. J., Axinte, R., Fischer, H., Petäjä, T., Nölscher, A., Williams, J., Hens, K., Harder, H., Martinez-Harder, M., Novelli, A., Kubistin, D., Bohn, B., and Lelieveld, J.: Insights into HOx and ROx chemistry in the

boreal forest via measurement of peroxyacetic acid, peroxyacetic nitric anhydride (PAN) and hydrogen peroxide, Atmos. Chem. Phys., 18, 13457-13479, doi:10.5194/acp-18-13457-2018, 2018.

Curtis, A. R., and Sweetenham, W. P.: Facsimile, Atomic Energy Research Establishment, Report R-12805, 1987, 1987.

Dee, D. P., Uppala, S. M., Simmons, A. J., Berrisford, P., Poli, P., Kobayashi, S., Andrae, U., Balmaseda, M. A., Balsamo, G., Bauer, P., Bechtold, P., Beljaars, A. C. M., van de Berg, L., Bidlot, J., Bormann, N., Delsol, C., Dragani, R., Fuentes, M., Geer, A. J., Haimberger, L., Healy, S. B., Hersbach, H., Hólm, E. V., Isaksen, L., Kållberg, P., Köhler, M., Matricardi, M., McNally, A. P., Monge-Sanz, B. M., Morcrette, J.-J., Park, B.-K., Peubey, C., de Rosnay, P., Tavolato, C., Thépaut, J.-N., and Vitart, F.: The ERA-Interim reanalysis: configuration and performance of the data assimilation system, Quarterly Journal of the Royal Meteorological Society, 137, 553-597, doi:10.1002/qj.828, 2011.

Eger, P. G., Schuladen, J., Sobanski, N., Fischer, H., Karu, E., Williams, J., Riva, M., Zha, Q., Ehn, M., Quéléver, L. L. J., Schallhart, S., Lelieveld, J., and Crowley, J. N.: Pyruvic acid in the boreal forest: gas-phase mixing ratios and impact on radical chemistry, Atmos. Chem. Phys., 20, 3697-3711, doi:10.5194/acp-20-3697-2020, 2020.

Eugene, A. J., Pillar, E. A., Colussi, A. J., and Guzman, M. I.: Enhanced Acidity of Acetic and Pyruvic Acids on the Surface of Water, Langmuir, 34, 9307-9313, doi:10.1021/acs.langmuir.8b01606, 2018.

Fischer, H., Axinte, R., Bozem, H., Crowley, J. N., Ernest, C., Gilge, S., Hafermann, S., Harder, H., Hens, K., Janssen, R. H. H., Königstedt, R., Kubistin, D., Mallik, C., Martinez, M., Novelli, A., Parchatka, U., Plass-Dülmer, C., Pozzer, A., Regelin, E., Reiffs, A., Schmidt, T., Schuladen, J., and Lelieveld, J.: Diurnal variability, photochemical production and loss processes of hydrogen peroxide in the boundary layer over Europe, Atmos. Chem. Phys., 19, 11953-11968, doi:10.5194/acp-19-11953-2019, 2019.

Gaona-Colman, E., Blanco, M. B., Barnes, I., Wiesen, P., and Teruel, M. A.: OH- and O-3-initiated atmospheric degradation of camphene: temperature dependent rate coefficients, product yields and mechanisms, Rsc Advances, 7, 2733-2744, doi:10.1039/c6ra26656h, 2017.

Grosjean, D.: Atmospheric reactions of ortho cresol: gas phase and aerosol products, Atmospheric Environment (1967), 18, 1641-1652, doi:10.1016/0004-6981(84)90386-X, 1984.

Grosjean, D., Williams, E. L., and Grosjean, E.: Atmospheric chemistry of isoprene and of its carbonyl products, Env. Sci. Tech., 27, 830-840, doi:10.1021/es00042a004, 1993.

Guenther, A. B., Zimmerman, P. R., Harley, P. C., Monson, R. K., and Fall, R.: ISOPRENE AND MONOTERPENE EMISSION RATE VARIABILITY - MODEL EVALUATIONS AND SENSITIVITY ANALYSES, J. Geophys. Res. - Atmos., 98, 12609-12617, doi:10.1029/93jd00527, 1993.

Hakola, H., Hellén, H., and Laurila, T.: Ten years of light hydrocarbons (C2–C6) concentration measurements in background air in Finland, Atmos. Env., 40, 3621-3630, doi:10.1016/j.atmosenv.2005.08.019, 2006.

Hallquist, M., Wenger, J. C., Baltensperger, U., Rudich, Y., Simpson, D., Claeys, M., Dommen, J., Donahue, N., George, C., and Goldstein, A.: The formation, properties and impact of secondary organic aerosol: current and emerging issues, Atmos. Chem. Phys., 9, 5155-5236, doi:10.5194/acp-9-5155-2009, 2009.

Hari, P., and Kulmala, M.: Station for Measuring Ecosystem–Atmosphere Relations (SMEAR II), Boreal Env. Res., 10, 315–322, doi:10.1007/978-94-007-5603-8_9, 2005.

https://doi.org/10.5194/acp-2020-975
Preprint. Discussion started: 20 October 2020

Helas, G., Bingemer, H., and Andreae, M. O.: Organic acids over equatorial Africa: Results from DECAFE 88, Journal of Geophysical Research: Atmospheres, 97, 6187-6193, doi:10.1029/91jd01438, 1992.

Hellén, H., Kouznetsov, R., Anttila, P., and Hakola, H.: Increasing influence of easterly air masses on NMHC concentrations at the Pallas-Sodankylä GAW station, 2015.

Hellén, H., Praplan, A. P., Tykkä, T., Ylivinkka, I., Vakkari, V., Bäck, J., Petäjä, T., Kulmala, M., and Hakola, H.: Long-term measurements of volatile organic compounds highlight the importance of sesquiterpenes for the atmospheric chemistry of a boreal forest, Atmos. Chem. Phys., 18, 13839-13863, doi:10.5194/acp-18-13839-2018, 2018.

IUPAC: Task Group on Atmospheric Chemical Kinetic Data Evaluation, (Ammann, M., Cox, R.A., Crowley, J.N., Herrmann, H., Jenkin, M.E., McNeill, V.F., Mellouki, A., Rossi, M. J., Troe, J. and Wallington, T. J.) http://iupac.pole-ether.fr/index.html., 2020.

Jacob, D. J., and Wofsy, S. C.: Photochemistry of biogenic emissions over the Amazon forest, J. Geophys. Res. -Atmos., 93, 1477-1486, doi:10.1029/JD093iD02p01477, 1988.

Jardine, K., Abrell, L., Kurc, S. A., Huxman, T., Ortega, J., and Guenther, A.: Volatile organic compound emissions from Larrea tridentata (creosotebush), Atmos. Chem. Phys., 10, 12191-12206, doi:10.5194/acp-10-12191-2010, 2010a.

Jardine, K. J., Sommer, E. D., Saleska, S. R., Huxman, T. E., Harley, P. C., and Abrell, L.: Gas Phase Measurements of Pyruvic Acid and Its Volatile Metabolites, Env. Sci. Tech., 44, 2454-2460, doi:10.1021/es903544p, 2010b.

Kanakidou, M., Seinfeld, J., Pandis, S., Barnes, I., Dentener, F., Facchini, M., Dingenen, R. V., Ervens, B., Nenes, A., and Nielsen, C.: Organic aerosol and global climate modelling: a review, Atmos. Chem. Phys., 5, 1053-1123, doi:10.5194/acp-5-1053-2005, 2005.

Liebmann, J., Karu, E., Sobanski, N., Schuladen, J., Ehn, M., Schallhart, S., Quéléver, L., Hellen, H., Hakola, H., Hoffmann, T., Williams, J., Fischer, H., Lelieveld, J., and Crowley, J. N.: Direct measurement of NO_3 radical reactivity in a boreal forest, Atmos. Chem. Phys., 2018, 3799-3815, doi:10.5194/acp-18-3799-2018, 2018.

Liebmann, J., Sobanski, N., Schuladen, J., Karu, E., Hellén, H., Hakola, H., Zha, Q., Ehn, M., Riva, M., Heikkinen, L., Williams, J., Fische, H., Lelieveld, J., and Crowley, J. N.: Alkyl nitrates in the boreal forest: formation via the NO3-, OH- and O3-induced oxidation of biogenic volatile organic compounds and ambient lifetimes, Atmos. Chem. Phys., 19, 10391-10403, doi:10.5194/acp-19-10391-2019, 2019.

Mellouki, A., and Mu, Y.: On the atmospheric degradation of pyruvic acid in the gas phase, Journal of Photochemistry and Photobiology A: Chemistry, 157, 295-300, doi:10.1016/S1010-6030(03)00070-4, 2003.

Millet, D. B., Guenther, A., Siegel, D. A., Nelson, N. B., Singh, H. B., de Gouw, J. A., Warneke, C., Williams, J., Eerdekens, G., and Sinha, V.: Global atmospheric budget of acetaldehyde: 3-D model analysis and constraints from in-situ and satellite observations, Atmos. Chem. Phys., 10, 3405-3425, doi:10.5194/acp-10-3405-2010, 2010.

Paulot, F., Crounse, J. D., Kjaergaard, H. G., Kroll, J. H., Seinfeld, J. H., and Wennberg, P. O.: Isoprene photooxidation: new insights into the production of acids and organic nitrates, Atmos. Chem. Phys., 9, 1479-1501, doi:10.5194/acp-9-1479-2009, 2009.

Perring, A. E., Pusede, S. E., and Cohen, R. C.: An observational perspective on the atmospheric impacts of alkyl and multifunctional nitrates on ozone and secondary organic aerosol, Chem. Rev., 113, 5848-5870, doi:doi:10.1021/cr300520x, 2013.

Petäjä, T., Mauldin, I. R. L., Kosciuch, E., McGrath, J., Nieminen, T., Paasonen, P., Boy, M., Adamov, A., Kotiaho, T., and Kulmala, M.: Sulfuric acid and OH concentrations in a boreal forest site, Atmos. Chem. Phys., 9, 7435-7448, doi:10.5194/acp-9-7435-2009, 2009.

Praplan, A. P., Hegyi-Gaeggeler, K., Barmet, P., Pfaffenberger, L., Dommen, J., and Baltensperger, U.: Online measurements of water-soluble organic acids in the gas and aerosol phase from the photooxidation of 1, 3, 5-trimethylbenzene, Atmos. Chem. Phys., 14, 8665-8677, doi:10.5194/acp-14-8665-2014, 2014.

Raber, W. H., and Moortgat, G. K.: Photooxidation of selected carbonyl compounds in air: methyl ethyl ketone, methyl vinyl ketone, methacrolein and methylglyoxal, Progress and problems in atmospheric chemistry, edited by: Barker, JR, World Scientific Publishing, Singapore, 318-373, 1995.

Reed Harris, A. E., Cazaunau, M., Gratien, A., Pangui, E., Doussin, J.-F., and Vaida, V.: Atmospheric Simulation Chamber Studies of the Gas-Phase Photolysis of Pyruvic Acid, J. Phys. Chem. A, 121, 8348-8358, doi:10.1021/acs.jpca.7b05139, 2017.

Rissanen, K., Vanhatalo, A., Salmon, Y., Bäck, J., and Hölttä, T.: Stem emissions of monoterpenes, acetaldehyde and methanol from Scots pine (Pinus sylvestris L.) affected by tree–water relations and cambial growth, Plant, Cell & Environment, doi:10.1111/pce.13778, 2020.

Roberts, J. M., Flocke, F., Chen, G., de Gouw, J., Holloway, J. S., Hübler, G., Neuman, J. A., Nicks Jr., D. K., Nowak, J. B., Parrish, D. D., Ryerson, T. B., Sueper, D. T., Warneke, C., and Fehsenfeld, F. C.: Measurement of peroxycarboxylic nitric anhydrides (PANs) during the ITCT 2K2 aircraft intensive experiment, Journal of Geophysical Research: Atmospheres, 109, doi:10.1029/2004jd004960, 2004.

Roiger, A., Aufmhoff, H., Stock, P., Arnold, F., and Schlager, H.: An aircraft-borne chemical ionization - ion trap mass spectrometer (CI-ITMS) for fast PAN and PPN measurements, Atmos. Meas. Tech., 4, 173-188, doi:doi:10.5194/amt-4-173-2011, 2011.

Shepson, P. B., Bottenheim, J. W., Hastie, D. R., and Venkatram, A.: Determination of the relative ozone and PAN deposition velocities at night, Geophys. Res. Lett., 19, 1121-1124, doi:10.1029/92gl01118, 1992a.

Shepson, P. B., Hastie, D. R., So, K. W., and Schiff, H. I.: Relationships between PAN, PPN and O_3 at urban and rural sites in ontario, Atmos. Env. A, 26, 1259-1270, doi:10.1016/0960-1686(92)90387-z, 1992b.

Stefan, M. I., and Bolton, J. R.: Reinvestigation of the acetone degradation mechanism in dilute aqueous solution by the UV/H2O2 process, Env. Sci. Tech., 33, 870-873, doi:10.1021/es9808548, 1999.

Talbot, R., Andreae, M., Berresheim, H., Jacob, D. J., and Beecher, K.: Sources and sinks of formic, acetic, and pyruvic acids over Central Amazonia: 2. Wet season, Journal of Geophysical Research: Atmospheres, 95, 16799-16811, doi:10.1029/JD095iD10p16799, 1990.

Walker, D.: Pyruvate carboxylation and plant metabolism, Biological Reviews, 37, 215-254, doi:10.1111/j.1469-185X.1962.tb01611.x, 1962.

Wang, N., Edtbauer, A., Stönner, C., Pozzer, A., Bourtsoukidis, E., Ernle, L., Dienhart, D., Hottmann, B., Fischer, H., Schuladen, J., Crowley, J. N., Paris, J. D., Lelieveld, J., and Williams, J.: Measurements of carbonyl compounds around the Arabian Peninsula indicate large missing sources of acetaldehyde, Atmos. Chem. Phys. Discuss., 2020, 1-30, doi:10.5194/acp-2020-135, 2020.

https://doi.org/10.5194/acp-2020-975
Preprint. Discussion started: 20 October 2020

Wang, S. Y., Hornbrook, R. S., Hills, A., Emmons, L. K., Tilmes, S., Lamarque, J. F., Jimenez, J. L., Campuzano-Jost, P., Nault, E. A., Crounse, J. D., Wennberg, P. O., Kim, M., Allen, H., Ryerson, T. B., Thompson, C. R., Peischl, J., Moore, F., Nance, D., Hall, B., Elkins, J., Tanner, D., Huey, L. G., Hall, S. R., Ullmann, K., Orlando, J. J., Tyndall, G. S., Flocke, F. M., Ray, E., Hanisco, T. F., Wolfe, G. M., St Clair, J., Commane, R., Daube, B., Barletta, B., Blake, D. R., Weinzierl, B., Dollner, M., Conley, A., Vitt, F., Wofsy, S. C., Riemer, D. D., and Apel, E. C.: Atmospheric acetaldehyde: importance of air-sea exchange and a missing source in the remote troposphere, Geophys. Res. Lett., 46, 5601-5613, doi:10.1029/2019gl082034, 2019.

Williams, J., Crowley, J., Fischer, H., Harder, H., Martinez, M., Petaja, T., Rinne, J., Back, J., Boy, M., Dal Maso, M., Hakala, J., Kajos, M., Keronen, P., Rantala, P., Aalto, J., Aaltonen, H., Paatero, J., Vesala, T., Hakola, H., Levula, J., Pohja, T., Herrmann, F., Auld, J., Mesarchaki, E., Song, W., Yassaa, N., Nolscher, A., Johnson, A. M., Custer, T., Sinha, V., Thieser, J., Pouvesle, N., Taraborrelli, D., Tang, M. J., Bozem, H., Hosaynali-Beygi, Z., Axinte, R., Oswald, R., Novelli, A., Kubistin, D., Hens, K., Javed, U., Trawny, K., Breitenberger, C., Hidalgo, P. J., Ebben, C. J., Geiger, F. M., Corrigan, A. L., Russell, L. M., Ouwersloot, H. G., de Arellano, J. V. G., Ganzeveld, L., Vogel, A., Beck, M., Bayerle, A., Kampf, C. J., Bertelmann, M., Kollner, F., Hoffmann, T., Valverde, J., Gonzalez, D., Riekkola, M. L., Kulmala, M., and Lelieveld, J.: The summertime Boreal forest field measurement intensive (HUMPPA-COPEC-2010): an overview of meteorological and chemical influences, Atmos. Chem. Phys., 11, 10599-10618, doi:10.5194/acp-11-10599-2011, 2011.

https://doi.org/10.5194/acp-2020-975
Preprint. Discussion started: 20 October 2020

Atmospheric Chemistry and Physics Discussions

Table 1: Overview of different model scenarios for pyruvic acid.

Scenario	ϕ	α_1	α_2	α_3	β	Dominant products	J_{pyr} [10^{-5} s^{-1}] (day / night)	k_{dep} [10^{-5} s^{-1}] (day / night)	k_{total} [10^{-5} s^{-1}] (day / night)	E_{pyr} / E_{MT} (average)
A	0	--	--	--	--	--	0 / 0	9 / 18	9 / 18	0.58
B	0.20	0.6	0.35	0.05	1	CH_3CHO	3 / 0	9 / 18	12 / 18	0.62
C	0.84	0.95	0	0.05	0.05	HO_2 + CH_3CO_3	12 / 0	9 / 18	21 / 18	0.74

ϕ = photolysis quantum yield, α_i and β are branching ratios forming the dominant products. k_i are loss rates of pyruvic acid, E_{pyr} / E_{MT} is the emission rate of pyruvic acid relative to MT.

Table 2: Emission rate of pyruvic acid (E_{pyr}) relative to isoprene (E_{iso}) and MT (E_{MT}), derived from different field and enclosure studies.

Reference	Location	Plant species	(E_{pyr} / E_{iso})	(E_{pyr} / E_{MT})
This study	Hyytiälä, Finland	Boreal forest	~ 20	0.62
Talbot et al. (1990)	Manaus, Brazil	Tropical forest	0.003	-
Jardine et al. (2010b)	Biosphere 2, Arizona, US	Tropical biome	0.17	4
Jardine et al. (2010b)	Biosphere 2, Arizona, US	Mango tree	0.05	1.7
Jardine et al. (2010a)	Biosphere 2, Arizona, US	Creosotebush	0.05	0.07

Table 3. Mean production rates of OH, HO_2, $CH_3C(O)O_2$, CH_3CHO and CH_3O_2 during IBAIRN and HUMPPA.

	Production rate in **IBAIRN** [10^5 molecule cm^{-3} s^{-1}]			Production rate in **HUMPPA** [10^5 molecule cm^{-3} s^{-1}]		
Scenario	**A**	**B**	**C**	**A**	**B**	**C**
OH	13.1	13.3	14.8	43.9	44.4	47.6
HO_2	5.8	5.9	7.9	34.7	35.6	41.7
CH_3CO_3	1.2	1.2	2.2	17.3	17.9	21.6
CH_3CHO	-	-	-	0.1	1.1	0.3
CH_3O_2	1.2	1.2	1.7	4.7	4.9	6.0

https://doi.org/10.5194/acp-2020-975
Preprint. Discussion started: 20 October 2020

Atmospheric Chemistry and Physics Discussions

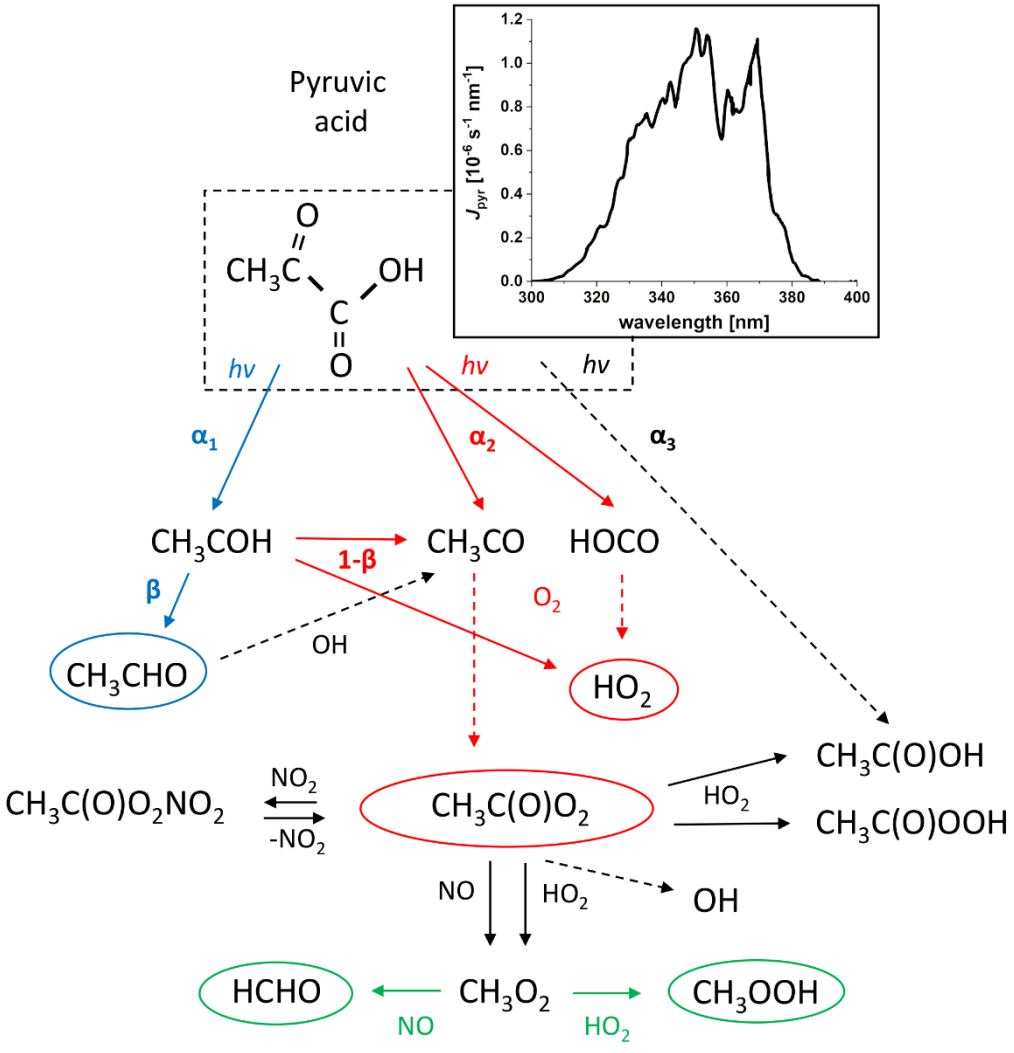

Figure 1: Radical and stable products from the photolysis of pyruvic acid (including branching ratios α_i and β) along with the wavelength resolved photolysis rates (J_{pyr} in units of 10^{-6} s^{-1} nm^{-1}) for 13.09.2016 at solar noon. J_{pyr} was calculated using a photolysis quantum yield of $\phi = 0.2$ and the absorption cross sections at 298 K preferred by IUPAC (2020).

https://doi.org/10.5194/acp-2020-975
Preprint. Discussion started: 20 October 2020

Atmospheric Chemistry and Physics Discussions

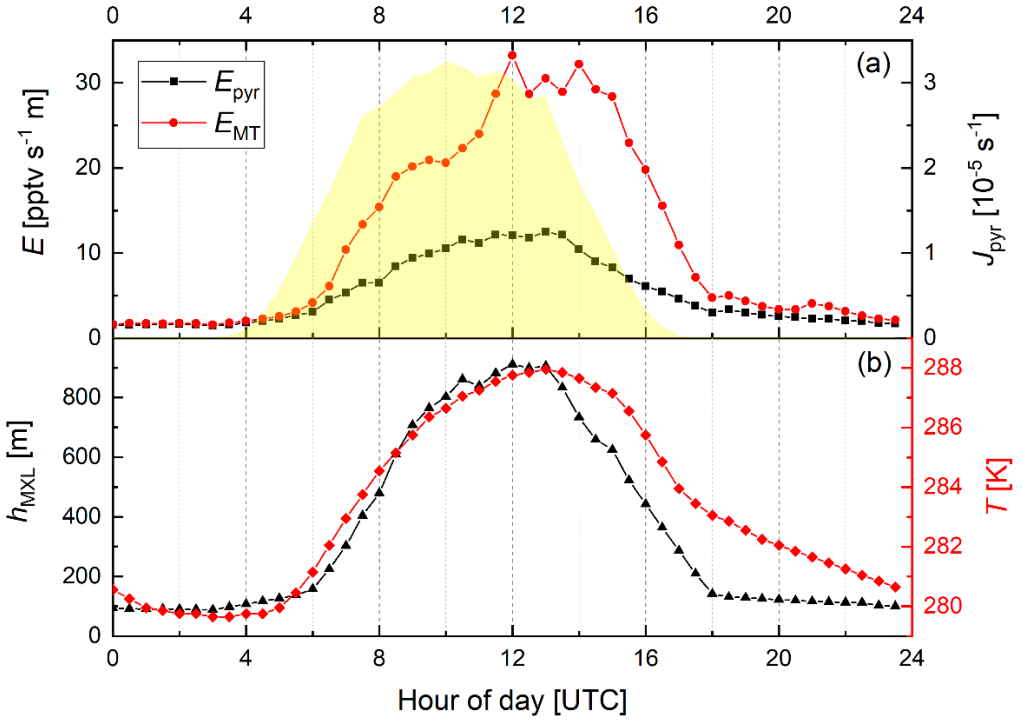

Figure 2: Diel variation of the (MXL height-corrected) emission rates of pyruvic acid (E_{pyr}, scenario B) and monoterpenes (E_{MT}) along with J_{pyr} (yellow shaded), T and h_{MXL} for the IBAIRN campaign.

5

https://doi.org/10.5194/acp-2020-975
Preprint. Discussion started: 20 October 2020

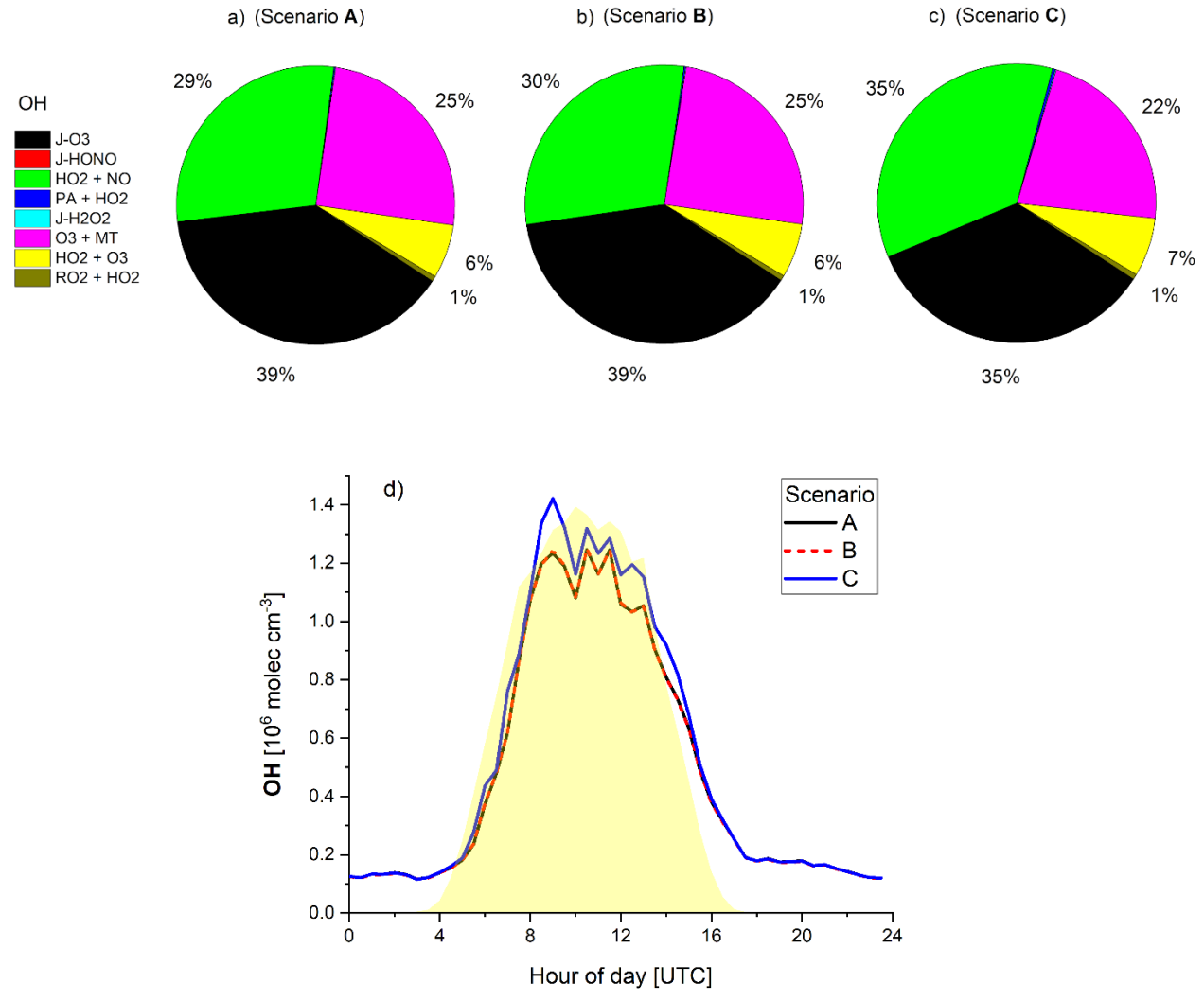

Figure 3: Modelled relative source strength (averaged throughout the diel cycle) and concentration of OH (along with the relative photolysis rate J_{pyr} in yellow) during IBAIRN using scenarios A, B and C (Table 1). *J* = photolysis; PA = peroxyacetyl radical; MT = sum of monoterpenes.

https://doi.org/10.5194/acp-2020-975
Preprint. Discussion started: 20 October 2020

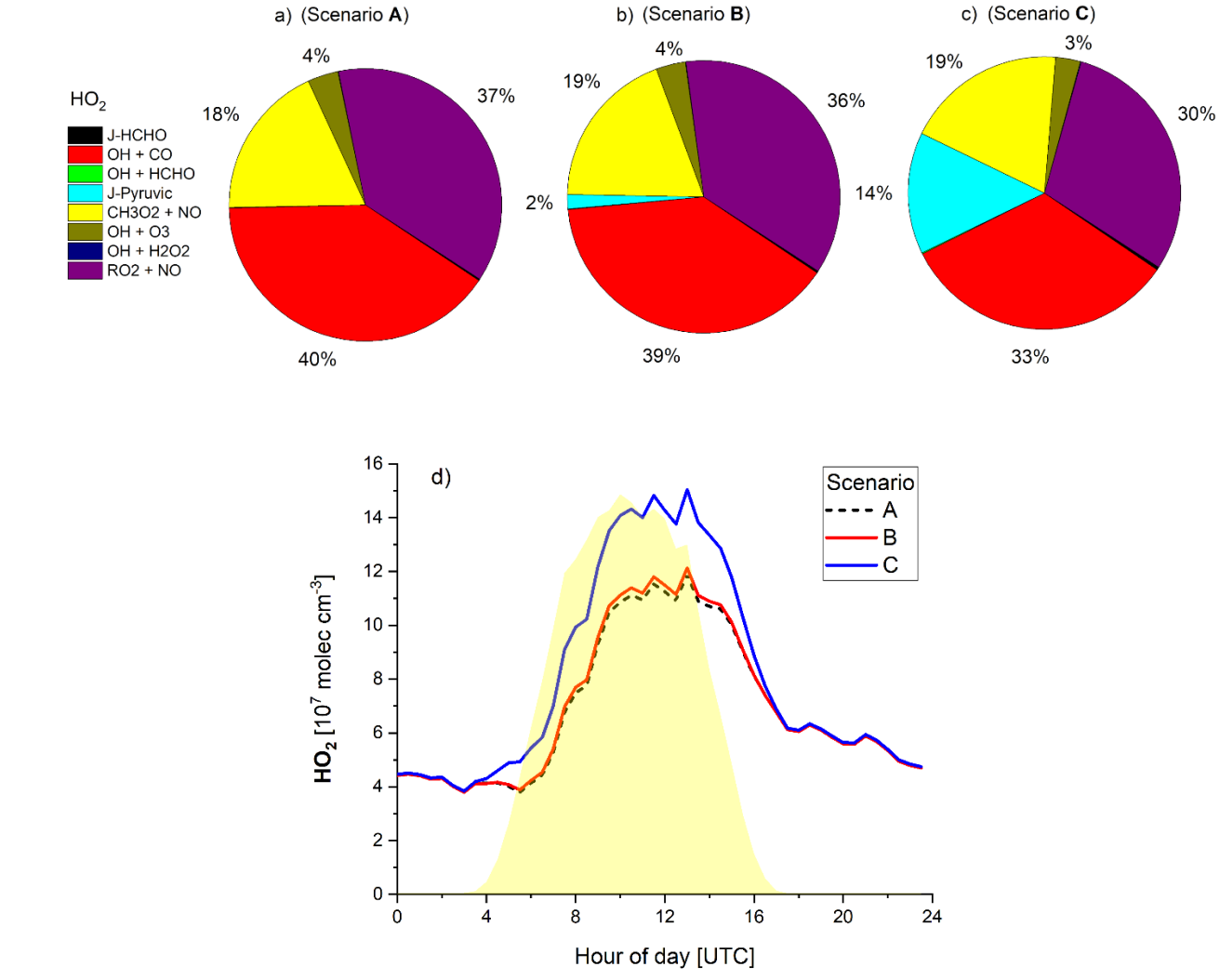

Figure 4: Modelled relative source strength (averaged throughout the diel cycle) and concentration of HO_2 (along with the relative photolysis rate J_{pyr} in yellow) during IBAIRN using scenarios A, B and C.

https://doi.org/10.5194/acp-2020-975
Preprint. Discussion started: 20 October 2020

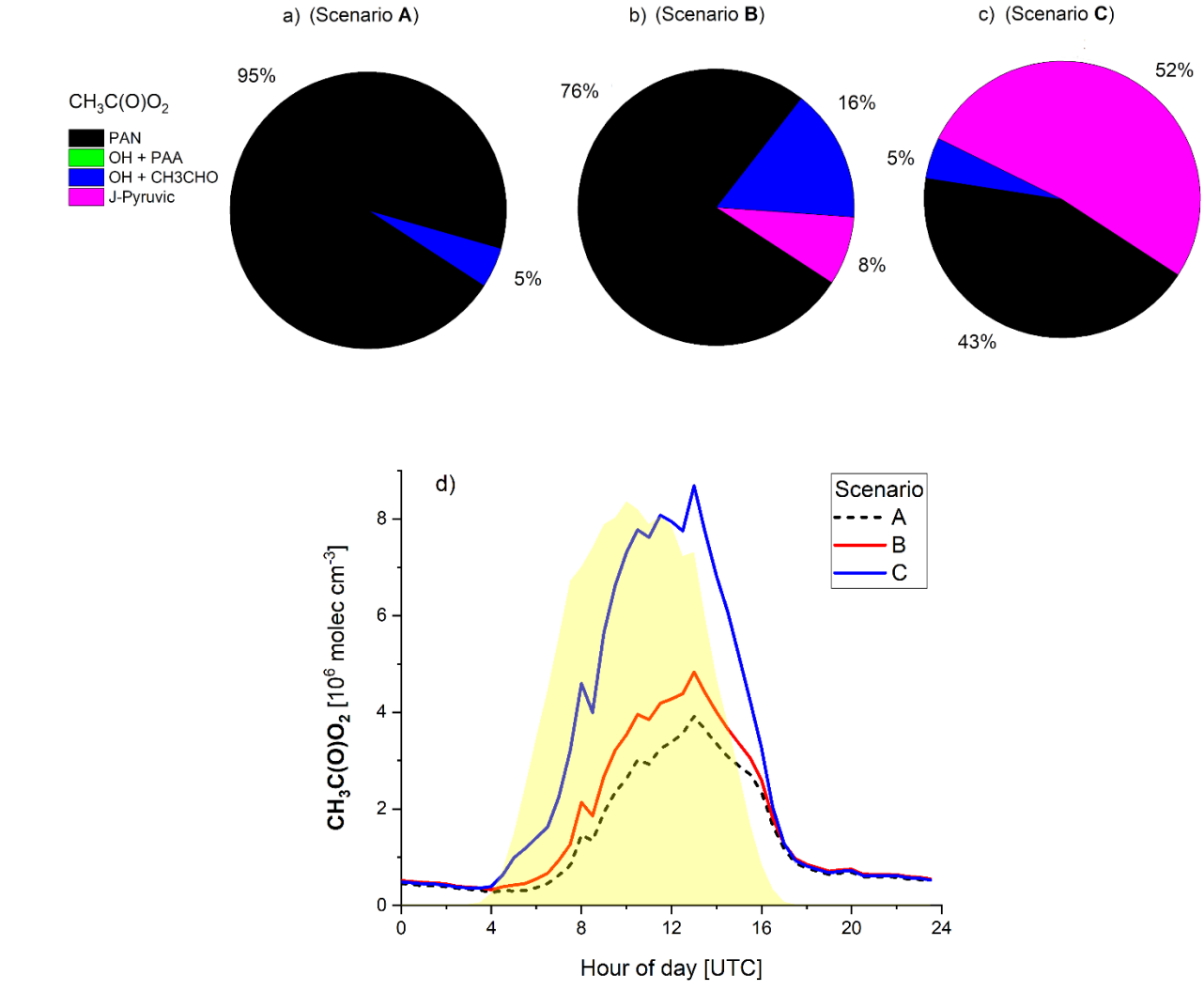

Figure 5: Modelled relative source strength (averaged throughout the diel cycle) and concentration of $CH_3C(O)O_2$ (along with the relative photolysis rate J_{pyr} in yellow) during IBAIRN using scenarios A, B and C.

https://doi.org/10.5194/acp-2020-975
Preprint. Discussion started: 20 October 2020

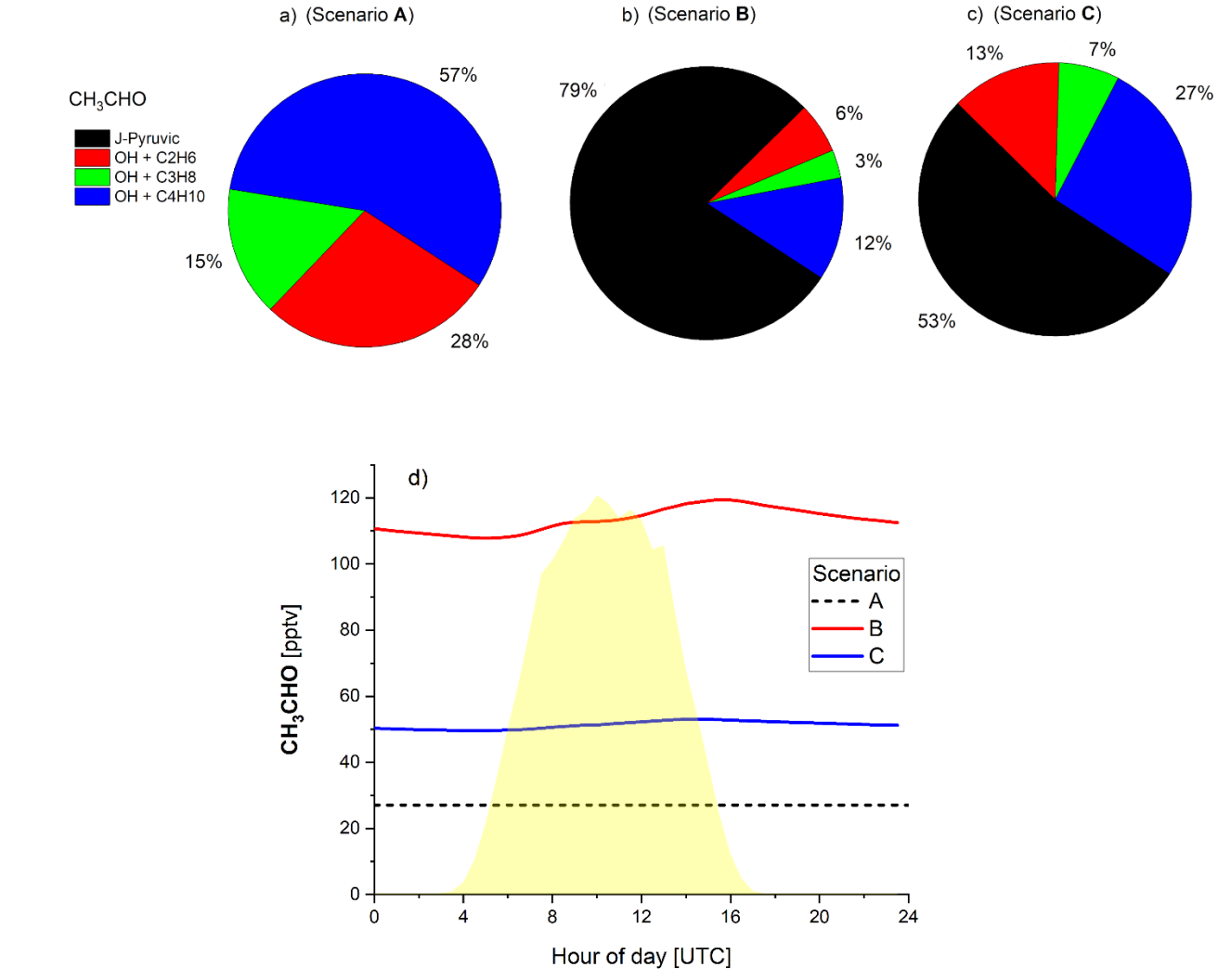

Figure 6: Modelled relative source strength (averaged throughout the diel cycle) and concentration of CH_3CHO (along with the relative photolysis rate J_{pyr} in yellow) during IBAIRN using scenarios A, B and C.

https://doi.org/10.5194/acp-2020-975
Preprint. Discussion started: 20 October 2020

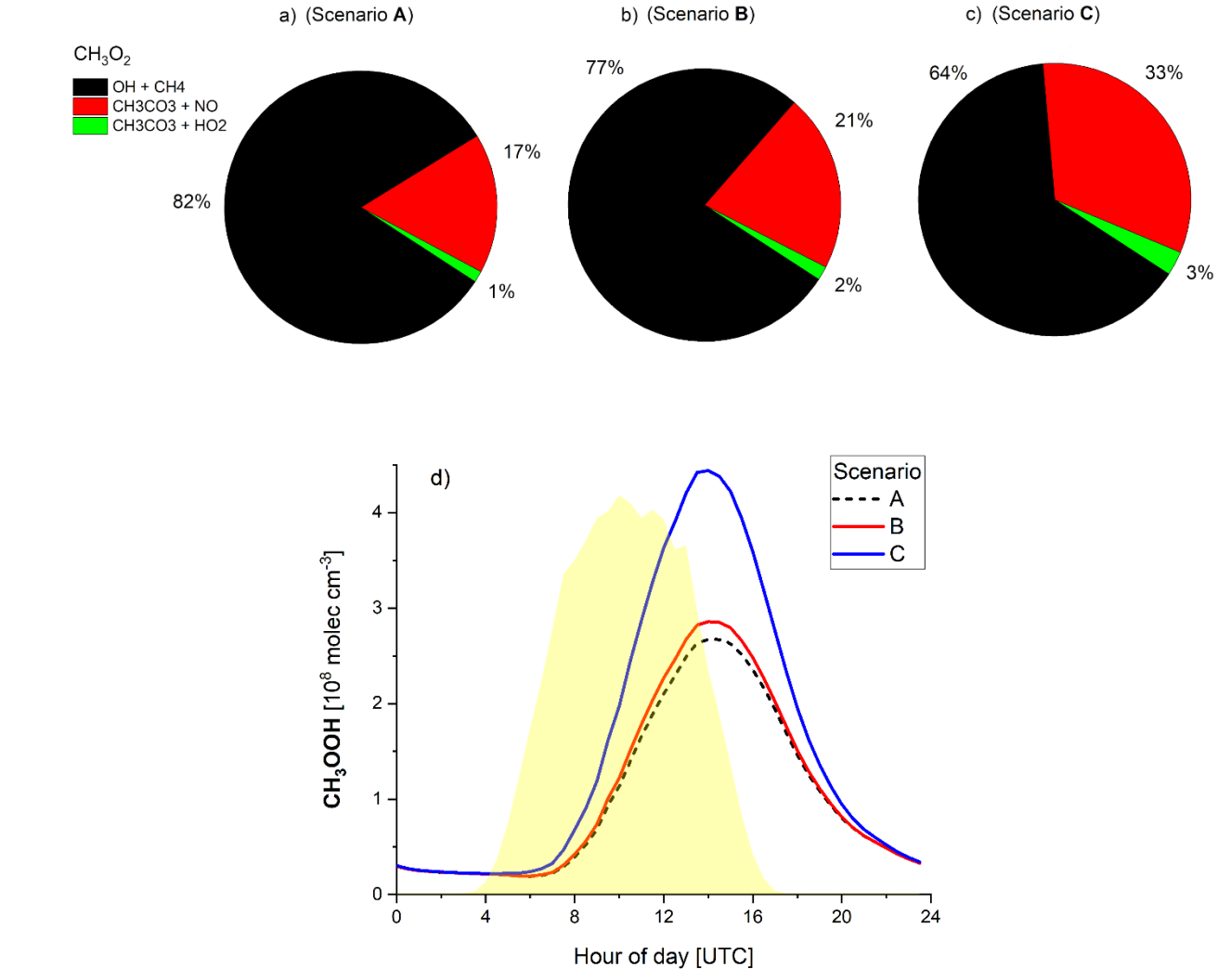

Figure 7: Modelled relative source strength (averaged throughout the diel cycle) of CH_3O_2 and concentration of CH_3OOH (along with the relative photolysis rate J_{pyr} in yellow) during IBAIRN using scenarios A, B and C.

https://doi.org/10.5194/acp-2020-975
Preprint. Discussion started: 20 October 2020

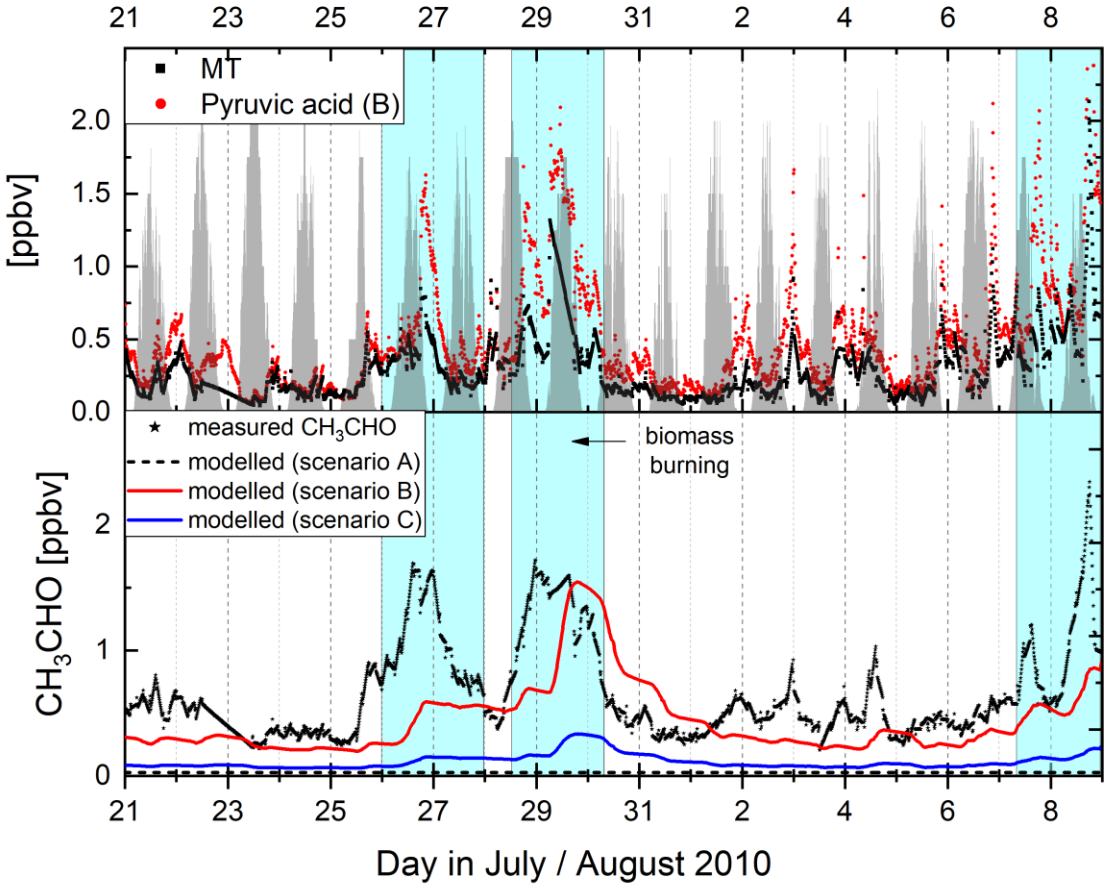

Figure 8: Upper panel: mixing ratio of MT (measured) and pyruvic acid (modelled, scenario B) during HUMPPA along with the photolysis rate J_{pyr} in grey. Lower panel: measured and modelled (scenarios A, B and C) acetaldehyde mixing ratios. Periods impacted by biomass burning plumes are highlighted in light blue.

https://doi.org/10.5194/acp-2020-975
Preprint. Discussion started: 20 October 2020

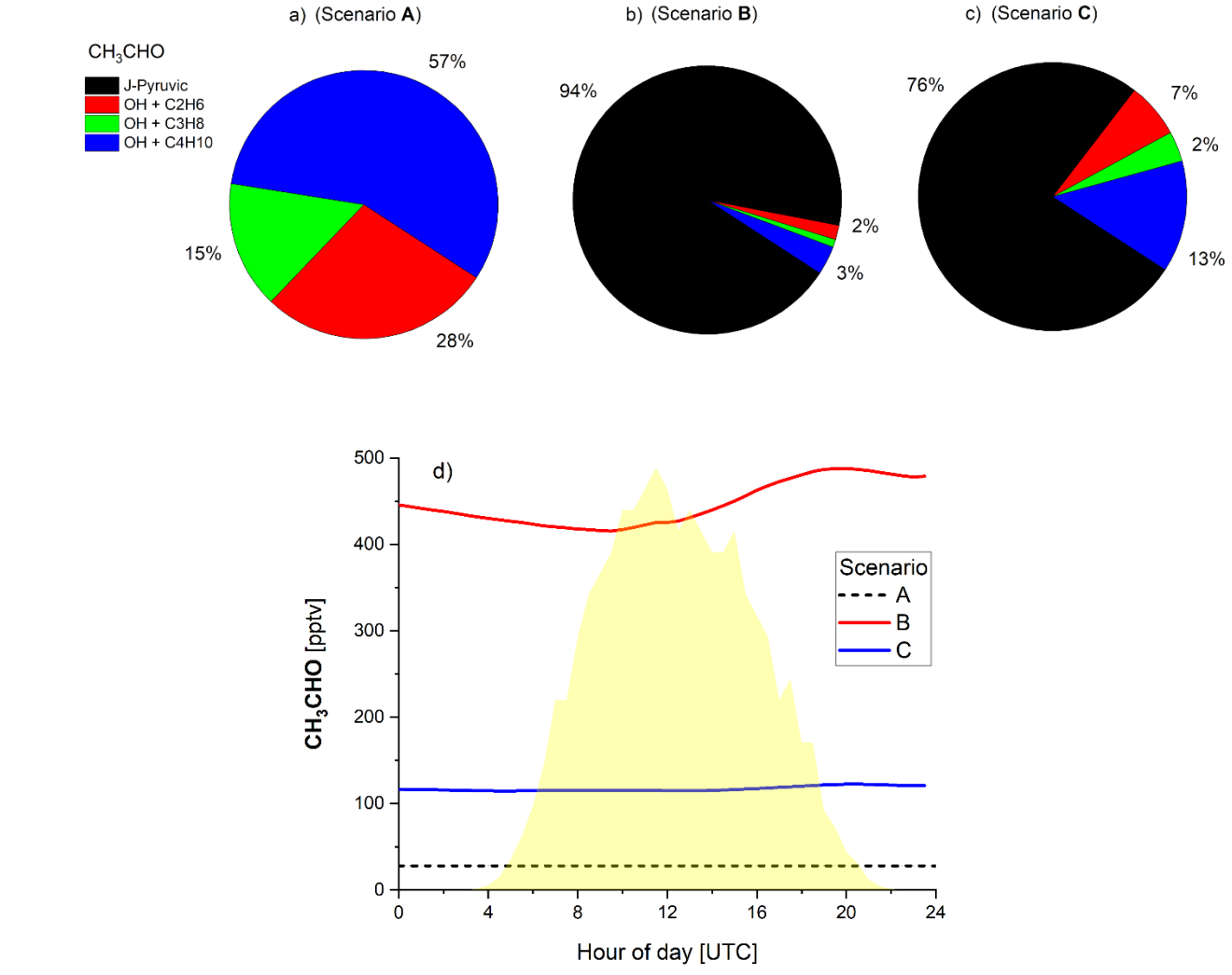

Figure 9: Modelled relative source strength (averaged throughout the diel cycle) and concentration of CH_3CHO during HUMPPA using scenarios A, B and C.

https://doi.org/10.5194/acp-2020-975
Preprint. Discussion started: 20 October 2020

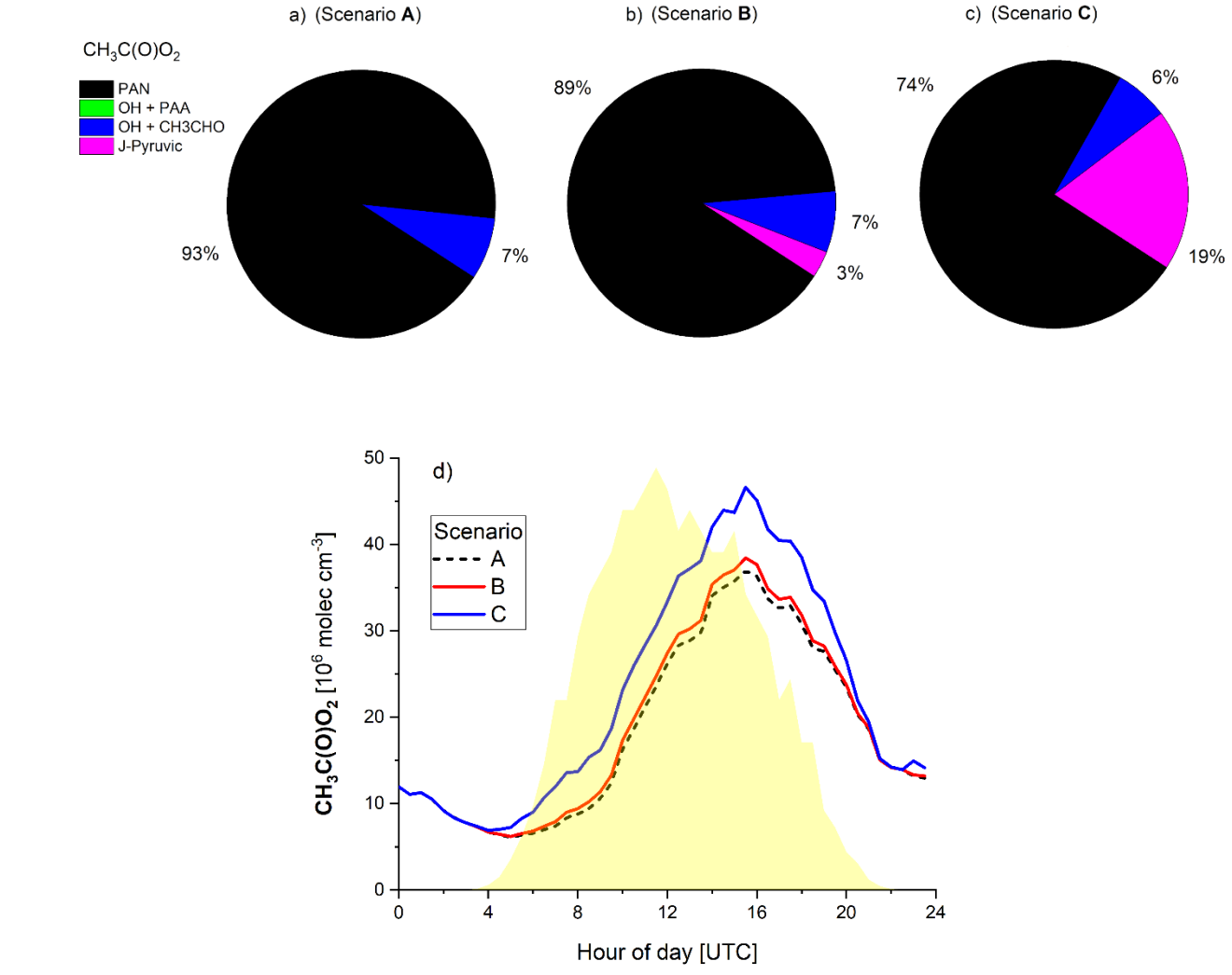

Figure 10: Modelled relative source strength (averaged throughout the diel cycle) and concentration of $CH_3C(O)O_2$ (along with the relative photolysis rate J_{pyr} in yellow) during HUMPPA using scenarios A, B and C.